catalysts

MDPI

*Article*

# Selective Catalytic Reduction of NO by $NH_3$ over Mn–Cu Oxide Catalysts Supported by Highly Porous Silica Gel Powder: Comparative Investigation of Six Different Preparation Methods

**Davyd Urbanas * and Edita Baltrėnaitė-Gedienė**

Faculty of Environmental Engineering, Vilnius Gediminas Technical University, Saulėtekio Ave. 11, LT-10223 Vilnius, Lithuania; edita.baltrenaite@vilniustech.lt
* Correspondence: davyd.urbanas@vilniustech.lt

**Abstract:** In this study, Mn-based catalysts supported by highly porous silica gel powder (SSA up to 470 $m^2 \cdot g^{-1}$ and total pore volume up to 0.8 $cm^3 \cdot g^{-1}$) were prepared by six different methods in liquid solutions (electroless metal deposition, stepwise addition of a reducing agent, wet impregnation, incipient wetness impregnation, urea hydrolysis, and ammonia evaporation) and tested for selective catalytic reduction of $NO_x$ with ammonia ($NH_3$-SCR de-$NO_x$). Prior to the activity test all the catalysts prepared were characterized by ICP-OES, SEM, EDX mapping, XPS, XRD and $N_2$ adsorption techniques to provide the comprehensive information about their composition and morphology, investigate the dispersion of active components on the carrier surface, identify the chemical forms and structural properties of the catalytically active species of the catalysts prepared. The results revealed that all the methods applied for preparation of SCR de-$NO_x$ catalysts can ensure the uniform distribution of Mn species on the carrier surface, however as it is typical for preparation techniques in a liquid phase the significant reduction in SSA and pore volume along with increasing the loading was observed. Considering both the physicochemical properties and the catalytic performance of the catalysts the least effective preparation method was shown to be ammonia evaporation, while the most attractive techniques are incipient wetness impregnation and electroless metal deposition.

**Keywords:** Mn-based oxide catalyst; silica gel powder; selective catalytic reduction; nitrogen oxide; electroless metal deposition; stepwise addition of a reducing agent; wet impregnation; incipient wetness impregnation; urea hydrolysis; ammonia evaporation



**Citation:** Urbanas, D.; Baltrėnaitė-Gedienė, E. Selective Catalytic Reduction of NO by $NH_3$ over Mn–Cu Oxide Catalysts Supported by Highly Porous Silica Gel Powder: Comparative Investigation of Six Different Preparation Methods. *Catalysts* **2021**, *11*, 702. https://doi.org/10.3390/catal11060702

Academic Editor: Leonarda Francesca Liotta

Received: 10 April 2021
Accepted: 28 May 2021
Published: 1 June 2021



## 1. Introduction

Nitrogen oxides ($NO_x$) are harmful and dangerous air pollutants for both the environment and human health. These compounds are generated as a result of fuel combustion and cause serious environmental problems, such as eutrophication, photochemical smog and acid rains [1,2]. The latter can lead to secondary negative changes in ecosystems such as the acidification of soil, rivers, and lakes. Atmospheric air with $NO_2$ concentrations above the limited value can irritate the human respiratory system and with the short-term exposure may increase the symptoms of respiratory diseases. The long-term exposure of the elevated concentrations of $NO_2$ in the ambient air can cause asthma and increased sensitivity to respiratory infections [3].

Catalytic removal of $NO_x$ from the flue gas, known as selective catalytic reduction with ammonia ($NH_3$-SCR de-$NO_x$), is considered to be the most efficient and attractive technique to reduce $NO_x$ emissions [4,5]. This technique provides the highest $NO_x$ conversion efficiency and does not cause secondary pollution or transfer of pollutants from one medium (air) to another (adsorbent/absorbent), since as a result of the catalytic reaction new harmless substances ($N_2$ and $H_2O$) are generated.

Considering that the energy production and distribution sector is a source of $NO_x$ emissions, significant interest has been focused on the development of low-temperature catalysts which can provide effective $NO_x$ conversion at the temperature range of 100–300 °C [6,7]. This is highly important for thermal power plants, where the tail-end SCR configuration is applied. In this case, the SCR reactor is placed downstream of all air pollution control equipment installed on a plant (i.e., particulate control and desulfurization equipment) [8].

Mn-based catalysts are known as the low-temperature catalysts for $NO_x$ conversion by ammonia [9–21]. Additionally, it is well-known that bimetallic and polymetallic oxide catalysts are more effective compared to the single-metal oxide catalysts [13,15,22–24]. Among the different transition metals, Cu was found to be an effective and economically feasible doping element of Mn-based SCR de-$NO_x$ catalysts [15,25,26]. In this study Mn–Cu active species were deposited on a highly porous support—silica gel 60 (powder with the size of 0.063–0.1 mm), possessing a high specific surface area of 470 $m^2 \cdot g^{-1}$ and high pore volume of 0.8 $cm^3 \cdot g^{-1}$, and the catalysts prepared were investigated for $NH_3$-SCR de-$NO_x$. The use of a porous support is highly important, as such a support provide the required surface area for a proper distribution of active species to be deposited. Higher $NO_x$ conversion efficiencies can be achieved via a larger distribution of the catalytically active species, as the agglomeration causes the decrease in the number of active sites available for the catalytic reaction. Another way to provide the required surface area for the deposition of active species is via the use of nanoparticles as a support. However, the application of nanoparticles, in the fluidized bed catalysts in particular, is highly problematic due to the significant agglomeration. The catalysts being investigated were prepared by six different methods: electroless metal deposition, stepwise addition of a reducing agent, wet impregnation, incipient wetness impregnation, urea hydrolysis, and ammonia evaporation. The aim of the study was to compare the abovementioned preparation methods by conducting the comprehensive investigation of both the physicochemical properties and the SCR performance of the catalysts prepared. Silica gel itself is not a favorable carrier for $NH_3$-SCR due to its low acidity, however it is suitable for the comparison of different techniques for the deposition of the catalytically active species on a highly porous support.

## 2. Results and Discussion

### *2.1. Catalyst Characterization*

#### 2.1.1. ICP-OES, SEM, EDX Elemental Mapping

Scanning electron microscopy (SEM) revealed that the silica gel powder is not stable in liquid solutions as it broke up into smaller pieces during the deposition process. The exception was the incipient wetness impregnation method, where the limited volume (equal to the total pore volume of the carrier) of the precursor solution was used. In all the catalysts prepared catalytically active species can be clearly observed from the SEM images (see Figure 1) excluding the sample prepared by the incipient wetness impregnation (IWI), since in the latter the active Mn–Cu species were mostly deposited inside the pores. The $Mn_{89.9}Cu_{10.1}/SiO_2$–AE catalyst was characterized by the obviously increased agglomeration, which was also proved by $N_2$ adsorption method demonstrated the significant reduction in the specific surface area and pore volume due to the pore clogging (see Section 2.1.2. Textural Properties). All the catalysts prepared were characterized by the same composition (ca. 90% of Mn and ca. 10% of Cu), however the loadings provided by the active species deposited were different for the different deposition methods applied (see Table 1). According to the ICP-OES results, the similar and the highest loadings were observed for the $Mn_{89.9}Cu_{10.1}/SiO_2$–AE and the $Mn_{91.1}Cu_{8.9}/SiO_2$–UH catalysts, however the urea hydrolysis method led to preparation of the catalyst characterized by better textural properties, in particular the specific surface area, total pore volume and average pore size, which all are important for the effective $NO_x$ catalytic conversion.

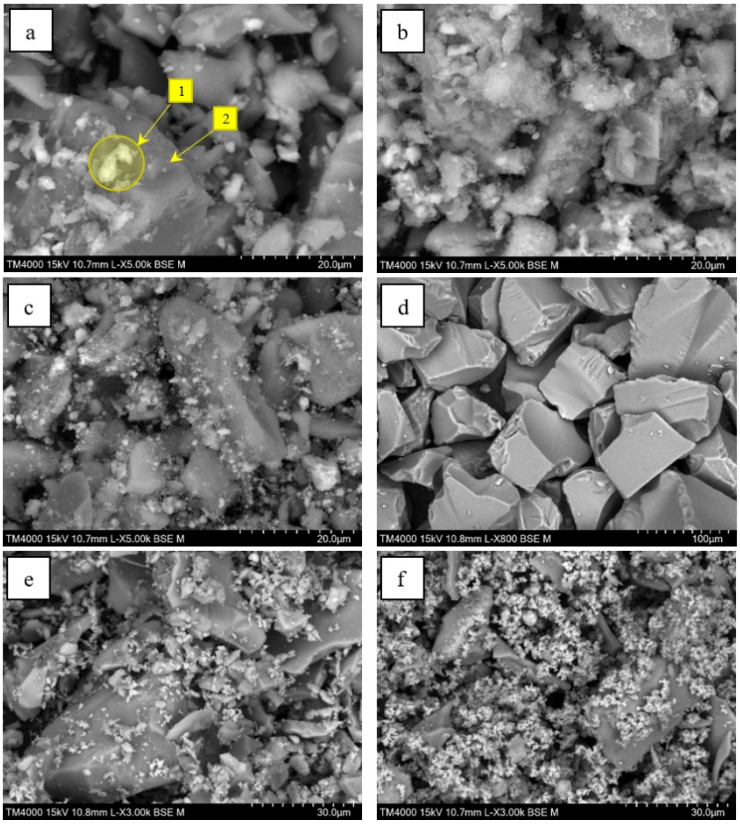


**Figure 1.** SEM images of the Mn–Cu oxide catalysts supported by the silica gel powder: $Mn_{90.8}Cu_{9.2}/SiO_2$–EMD (**a**); $Mn_{90.6}Cu_{9.4}/SiO_2$–SARA (**b**); $Mn_{90.9}Cu_{9.1}/SiO_2$–WI (**c**); $Mn_{91.1}Cu_{8.9}/SiO_2$–IWI (**d**); $Mn_{91.1}Cu_{8.9}/SiO_2$–UH (**e**) and $Mn_{89.9}Cu_{10.1}/SiO_2$–AE (**f**); 1—active species; 2—silica gel powder (carrier).

**Table 1.** Composition of the active catalytic layer deposited on the silica gel powder by different chemical methods in a liquid phase and the loading provided by the active components (based on ICP-OES analysis).

| Active Component | Share in the Catalytic Layer, wt% | Loading in the Supported Catalyst, wt% |
|---|---|---|
| | $Mn_{90.8}Cu_{9.2}/SiO_2$–EMD | |
| Mn | 90.8 | 3.5 |
| Cu | 9.2 | 0.4 |
| | $Mn_{90.6}Cu_{9.4}/SiO_2$–SARA | |
| Mn | 90.6 | 4.8 |
| Cu | 9.4 | 0.5 |
| | $Mn_{90.9}Cu_{9.1}/SiO_2$–WI | |
| Mn | 90.9 | 8.7 |
| Cu | 9.1 | 0.9 |
| | $Mn_{91.1}Cu_{8.9}/SiO_2$–IWI | |
| Mn | 91.1 | 1.1 |
| Cu | 8.9 | 0.1 |

**Table 1.** *Cont.*

| Active Component | Share in the Catalytic Layer, wt% | Loading in the Supported Catalyst, wt% |
|---|---|---|
| | $Mn_{91.1}Cu_{8.9}/SiO_2$–UH | |
| Mn | 91.1 | 11.1 |
| Cu | 8.9 | 1.1 |
| | $Mn_{89.9}Cu_{10.1}/SiO_2$–AE | |
| Mn | 89.9 | 13.3 |
| Cu | 10.1 | 1.5 |

The dispersion of the catalytically active species (Mn and Cu) on the surface of the silica gel powder is presented in Figure 2. As it can be seen, the main active component (Mn) was well-distributed throughout the surface, while some nonuniformity can be observed for the Cu species. Copper was used as a doping element, and it was deposited on the bare silica gel powder prior to the manganese species. The reason of slightly nonuniform distribution of Cu remained unclear and needs further understanding.

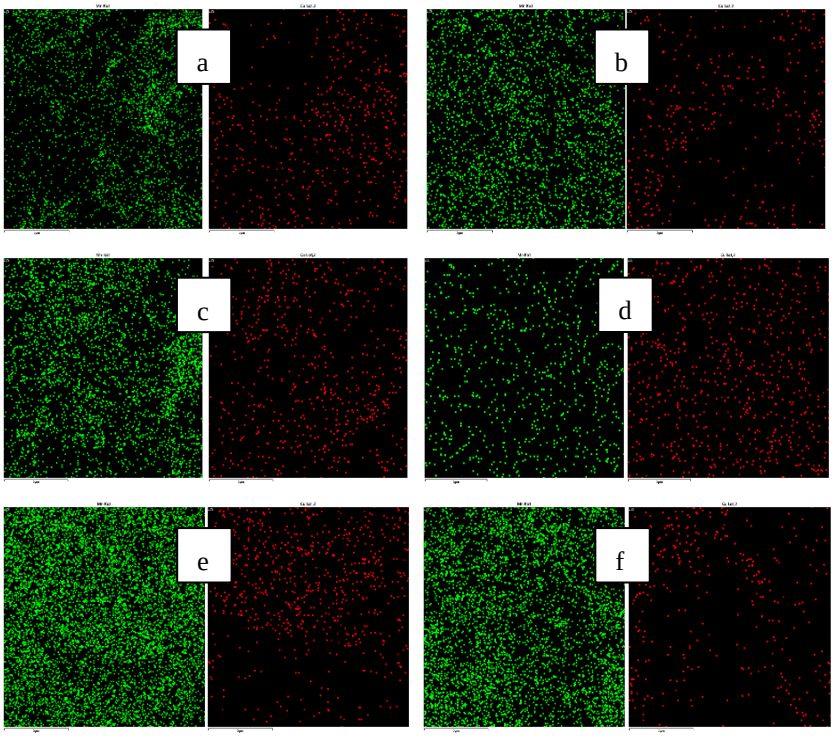


**Figure 2.** EDX mapping images of the Mn–Cu oxide catalysts supported by the silica gel powder (Mn—green; Cu—red): $Mn_{90.8}Cu_{9.2}/SiO_2$–EMD (**a**); $Mn_{90.6}Cu_{9.4}/SiO_2$–SARA (**b**); $Mn_{90.9}Cu_{9.1}/SiO_2$–WI (**c**); $Mn_{91.1}Cu_{8.9}/SiO_2$–IWI (**d**); $Mn_{91.1}Cu_{8.9}/SiO_2$–UH (**e**) and $Mn_{89.9}Cu_{10.1}/SiO_2$–AE (**f**).

### 2.1.2. Textural Properties

Textural properties of the catalysts prepared are presented in Table 2. As it mentioned before, different preparation methods applied resulted in different loadings of the active species deposited on the silica gel powder. This in turn led to different textural properties since such properties as SSA, pore volume and pore size strongly depend on loading. However, it was observed that the method applied can also impact the textural properties of the catalysts. As it can be seen from the Table 2, BET specific surface area and pore volume are in high correlation with Mn and Cu loading (correlation coefficient was equal to −0.84 and −0.96 for SSA and pore volume, respectively). At first, this can be explained by the fact that deposited materials fill the pores and reduce the SSA. However, from the

pore size distribution (see Figure 4) it can be supposed that the textural properties of all the catalysts prepared, except for the $Mn_{91.1}Cu_{8.9}/SiO_2$–IWI and $Mn_{90.8}Cu_{9.2}/SiO_2$–EMD catalysts, are mainly provided by the active species deposited. In this case the decrease in SSA and pore volume along with increase in loading can by assigned to agglomeration: the higher the loading, the higher the agglomeration of active species. However, the catalyst prepared by the urea hydrolysis method ($Mn_{91.1}Cu_{8.9}/SiO_2$–UH) was out of this trend, since with loading 1.3-times higher than that of the $Mn_{90.9}Cu_{9.1}/SiO_2$–WI catalyst it showed 1.6-times higher SSA. This can be explained by both the pore size and the pore volume of the $Mn_{91.1}Cu_{8.9}/SiO_2$–UH catalyst, which were 2-times and 1.2-times smaller, respectively, than that of the $Mn_{90.9}Cu_{9.1}/SiO_2$–WI catalyst. The results revealed that based on the textural properties wet impregnation method is definitely not the optimal method for preparation of catalysts. The only obvious advantage of this method is its simplicity. However, to provide the final conclusions, the other parameters such as structural and chemical properties, as well as catalytic performance were further investigated.

**Table 2.** Textural properties and the total metal loading of the Mn–Cu oxide catalyst supported by the silica gel powder (based on the $N_2$ adsorption analysis).

| Sample | Textural Properties | | | Total (Mn + Cu) Loading, % |
|---|---|---|---|---|
| | BET SSA, $m^2 \cdot g^{-1}$ | Pore Volume, $cm^3 \cdot g^{-1}$ | Average Pore Size, nm | |
| Silica gel powder | 474 | 0.8 | 6.5 | 0 |
| $Mn_{91.1}Cu_{8.9}/SiO_2$–IWI | 251 | 0.62 | 8.6 | 1.2 |
| $Mn_{90.8}Cu_{9.2}/SiO_2$–EMD | 196 | 0.63 | 11.4 | 3.9 |
| $Mn_{90.6}Cu_{9.4}/SiO_2$–SARA | 61 | 0.44 | 35.3 | 5.3 |
| $Mn_{91.1}Cu_{8.9}/SiO_2$–UH | 50 | 0.27 | 22 | 12.2 |
| $Mn_{90.9}Cu_{9.1}/SiO_2$–WI | 32 | 0.22 | 43.6 | 9.6 |
| $Mn_{89.9}Cu_{10.1}/SiO_2$–AE | 0.9 | 0.01 | 82.6 | 14.8 |

The catalyst prepared by the ammonia evaporation method ($Mn_{89.9}Cu_{10.1}/SiO_2$–AE) was characterized by extremely low SSA (less than 1 $m^2 \cdot g^{-1}$), pore volume and large average pore size. Although the loading of this catalyst was the highest among all the catalysts prepared, it was only 1.2-times higher compared to the $Mn_{91.1}Cu_{8.9}/SiO_2$–UH catalyst being characterized by 50-times higher SSA and 27-times higher pore volume. Therefore, the ammonia evaporation method cannot be considered as the optimal preparation technique as well. The extremely low SSA and pore volume of the catalyst prepared by this method can be explained by clogging the pores of the carrier and significant agglomeration. The enhanced agglomeration was also shown by SEM images (see Figure 1). Li et al. [27] showed the opposite results, where the catalyst prepared by the ammonia evaporation method possessed even higher SSA compared to the support, and exhibited better textural properties than the catalysts prepared by impregnation and deposition precipitation techniques. At the same time, the predominance of the ammonia evaporation technique over the urea hydrolysis in terms of dispersion of active species on the carrier surface can be found in [28]. However, it is difficult to compare the results obtained in the present work with that existing in the literature as there are too many differences, such as different active species to be deposited and their precursors, different carriers used for the deposition, and different additional chemical reagents used during the deposition process. All these parameters can affect the textural properties of the catalysts prepared.

Considering the textural properties, the catalyst prepared by urea hydrolysis ($Mn_{91.1}Cu_{8.9}/SiO_2$–UH) can be considered as more attractive than the catalyst prepared by stepwise addition of a reducing agent ($Mn_{90.6}Cu_{9.4}/SiO_2$–SARA) since it has 2.3-times higher loading, however its SSA is only 1.2-times lower. This can be explained by the average pore size of the $Mn_{91.1}Cu_{8.9}/SiO_2$–UH catalyst, which is much lower compared to

that of the $Mn_{90.6}Cu_{9.4}/SiO_2$–SARA catalyst (see Table 2). However, to provide final conclusions on that which catalyst is more suitable for SCR the other properties and especially catalytic performance should be investigated.

According to the average pore size all the catalysts prepared can be assigned to mesoporous materials as the silica gel powder itself, except for the $Mn_{89.9}Cu_{10.1}/SiO_2$–AE catalyst, which was related to macroporous materials based on the IUPAC classification [29]. The adsorption/desorption isotherms of the catalysts prepared are depicted in Figure 3. According to the IUPAC classification the adsorption/desorption isotherms of the $Mn_{91.1}Cu_{8.9}/SiO_2$–IWI and the $Mn_{90.8}Cu_{9.2}/SiO_2$–EMD catalysts can be assigned to the type V with the hysteresis loop of H1 type, which is typical for mesoporous materials possessing well-defined cylindrical-like pores. The adsorption/desorption isotherms of the other catalysts more likely can be attributed to the type II, although the desorption isotherm does not coincide with the adsorption isotherm. The type II isotherms are typical for adsorption on macroporous materials with strong adsorbent-adsorbate interactions [30].

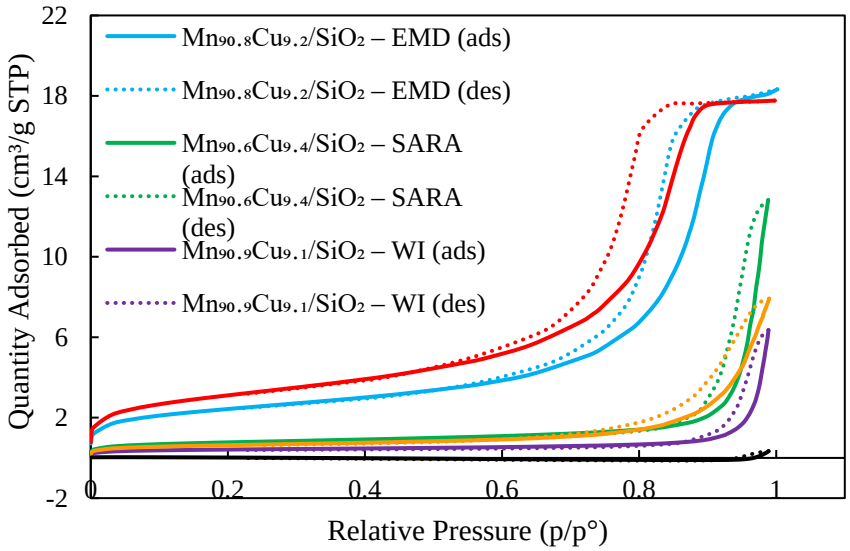


**Figure 3.** Nitrogen adsorption(ads)/desorption(des) isotherms of the Mn–Cu oxide catalysts supported by the silica gel powder.

Although according to the average pore size all the catalysts excluding the $Mn_{89.9}Cu_{10.1}/SiO_2$–AE were assigned to the mesoporous materials, the amount of macropores was significant for $Mn_{90.6}Cu_{9.4}/SiO_2$–SARA, $Mn_{90.9}Cu_{9.1}/SiO_2$–WI and $Mn_{91.1}Cu_{8.9}/SiO_2$–UH catalysts (Figure 4), which can explain the shape of the adsorption/desorption isotherms. The hysteresis loop of the type II isotherms can be defined as H3, meaning that the catalysts assigned to this isotherm type can be characterized by the slit-shaped pores [29,31]. From the Figure 4 it can be seen that the catalysts prepared by EMD and IWI methods have more or less similar pore size distribution to that of the silica gel powder. However, other catalysts are characterized by the significant changes in pore distribution after the deposition of active species and such catalysts possess much lower volume occupied by pores with the size lower than 25 nm, and huge amount of much larger pores. This is obviously related to the loading provided by the Mn and Cu species deposited, however the method applied also has the significant impact on the pore distribution. The pore size distribution data allow the assumption that pores of the $Mn_{90.6}Cu_{9.4}/SiO_2$–SARA, $Mn_{90.9}Cu_{9.1}/SiO_2$–WI $Mn_{91.1}Cu_{8.9}/SiO_2$–UH, and $Mn_{89.9}Cu_{10.1}/SiO_2$–AE catalysts are mainly the pores of the active species deposited on the carrier surface, rather than the pores of the carrier itself. The smaller pores mean higher SSA at the same total pore volume. Although the SSA of the $Mn_{90.6}Cu_{9.4}/SiO_2$–SARA catalyst is slightly higher than that of the $Mn_{91.1}Cu_{8.9}/SiO_2$–UH catalyst, this is only due to the lower loading and consequently higher total pore volume,

since in the latter there is much higher volume occupied by the pores with the size lower than 25 nm (see Figure 4).

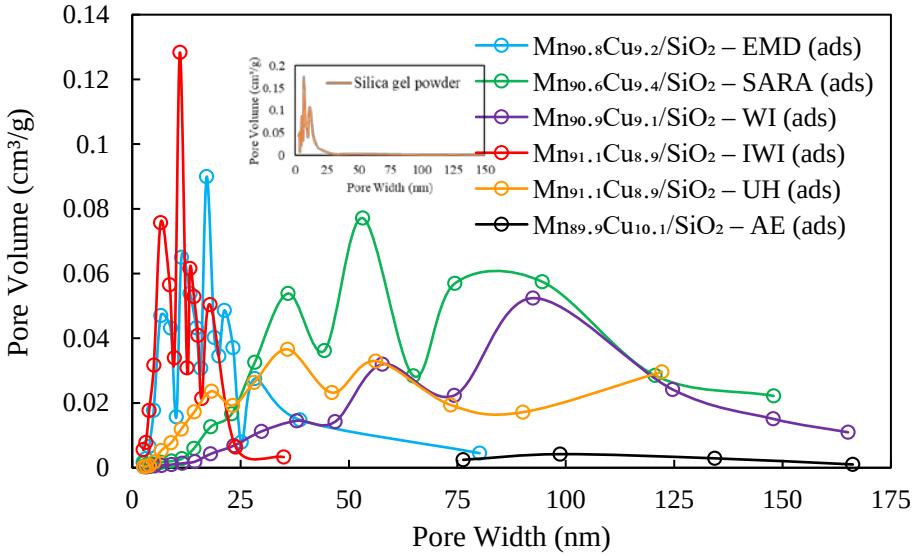


**Figure 4.** Pore distribution of the Mn–Cu oxide catalysts supported by the silica gel powder.

Therefore, the data of pore size distribution additionally demonstrated the predominance of the textural properties of the catalyst prepared by urea hydrolysis technique compared to that of catalysts prepared by stepwise addition of a reducing agent. It can also be clearly seen that the $Mn_{90.9}Cu_{9.1}/SiO_2$–WI catalyst possesses much higher volume occupied by the larger pores compared to the $Mn_{91.1}Cu_{8.9}/SiO_2$–UH catalyst, and therefore, although its loading is lower, it still possesses lower SSA. Thus, considering the textural properties, the urea hydrolysis technique is obviously more preferable compared to both wet impregnation and stepwise addition of a reducing agent. However, it was difficult to provide any reliable comparison between such preparation techniques as urea hydrolysis, electroless metal deposition and incipient wetness impregnation based on the textural properties due to the huge difference in loading.

### 2.1.3. XPS Analysis

Mn2p and O1s XPS spectra for all the Mn–Cu oxide catalysts supported by the silica gel powder are presented in Figures 5 and 6. The oxidation state of Cu was not under consideration since this element was used as the doping element and its loading was quite low for precise identification in most of the catalysts. Based on the XPS results it was supposed that Mn in all the catalysts prepared exists in $Mn^{3+}$ and $Mn^{4+}$ oxidation states with the predominance of the latter (see Figures 5 and 6 and Table 3).

**Table 3.** Binding energies and the corresponding oxidation states of Mn2p XPS spectra for the prepared Mn-based catalysts.

| Catalyst | Mn2p3/2, eV Peak | | $Mn^{4+} / \sum_{n=0}^{4} Mn^{n+}$ | Reference |
|---|---|---|---|---|
| | $Mn^{4+}$ ($Mn^{4+}$ Satellite) | $Mn^{3+}$ | | |
| $Mn_{91.1}Cu_{8.9}/SiO_2$–IWI | 642.4, (643.8) | 641.1 | 0.70 | [32–34] |
| $Mn_{90.8}Cu_{9.2}/SiO_2$–EMD | 642.5, (644.3) | 640.8 | 0.78 | [32–35] |
| $Mn_{90.6}Cu_{9.4}/SiO_2$–SARA | 642.9, (644.7) | 641.3 | 0.79 | [33,34,36] |
| $Mn_{91.1}Cu_{8.9}/SiO_2$–UH | 642.7, (644.4) | 641.2 | 0.69 | [33,34] |
| $Mn_{90.9}Cu_{9.1}/SiO_2$–WI | 642.6, (644.5) | 641.5 | 0.72 | [33,34] |
| $Mn_{89.9}Cu_{10.1}/SiO_2$–AE | 642.4, (643.9) | 641.1 | 0.81 | [33,34] |

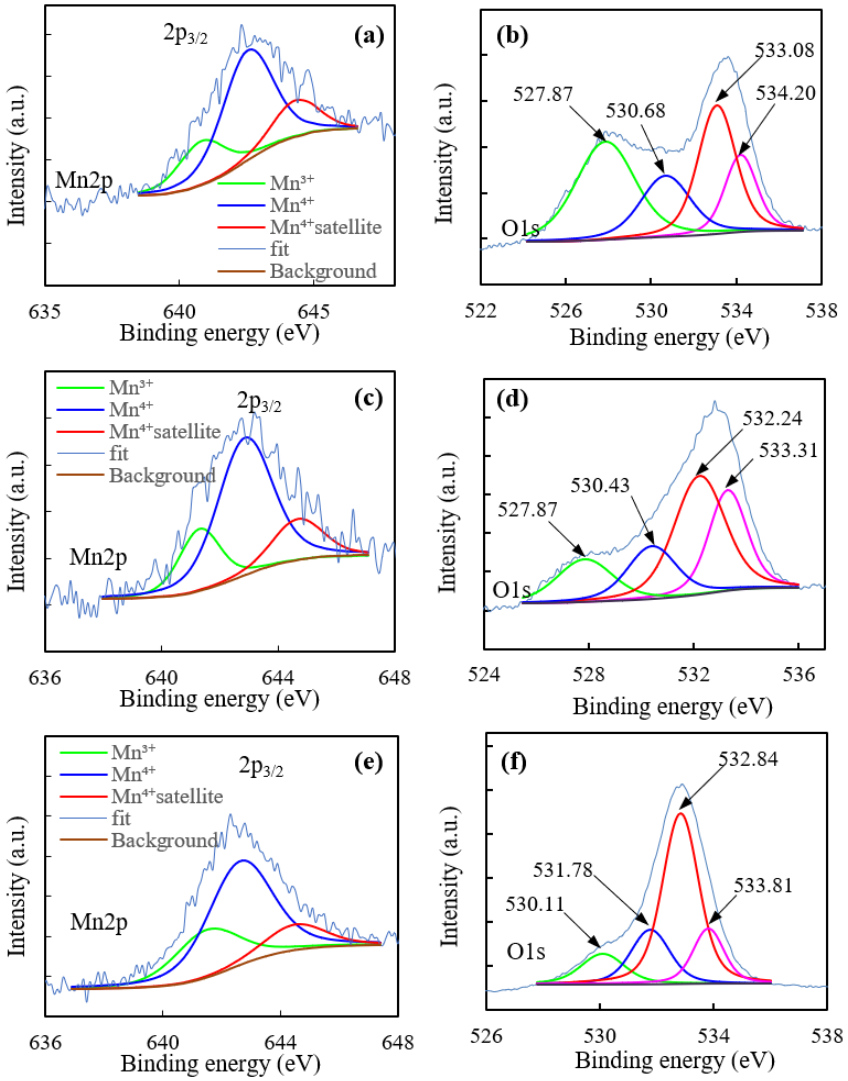


**Figure 5.** Mn2p and O1s XPS spectra for the $Mn_{90.8}Cu_{9.2}/SiO_2$–EMD (**a**,**b**); $Mn_{90.6}Cu_{9.4}/SiO_2$–SARA (**c**,**d**); and $Mn_{90.9}Cu_{9.1}/SiO_2$–WI (**e**,**f**) catalysts calcined at 350 °C for 3.5 h.

As it can be found in the literature, the higher the oxidation state of Mn in catalysts, the higher NO conversion efficiency can be achieved, and the $Mn^{4+}$ is considered to be most effective oxidation state of manganese among $Mn^{2+}$, $Mn^{3+}$, and $Mn^{4+}$ [9,36]. Table 3 demonstrates that all the catalysts prepared possess relatively high $Mn^{4+}/\sum_{n=0}^{4} Mn^{n+}$ ratio (from 0.7 to 0.8). For instance, this value in [36] varies in the range of 0.23–0.42. Based on the XPS results the highest $Mn^{4+}/\sum_{n=0}^{4} Mn^{n+}$ ratio was observed for the catalysts prepared by electroless metal deposition, stepwise addition of a reducing agent and ammonia evaporation techniques, however the difference observed between all the catalysts investigated was not significant.

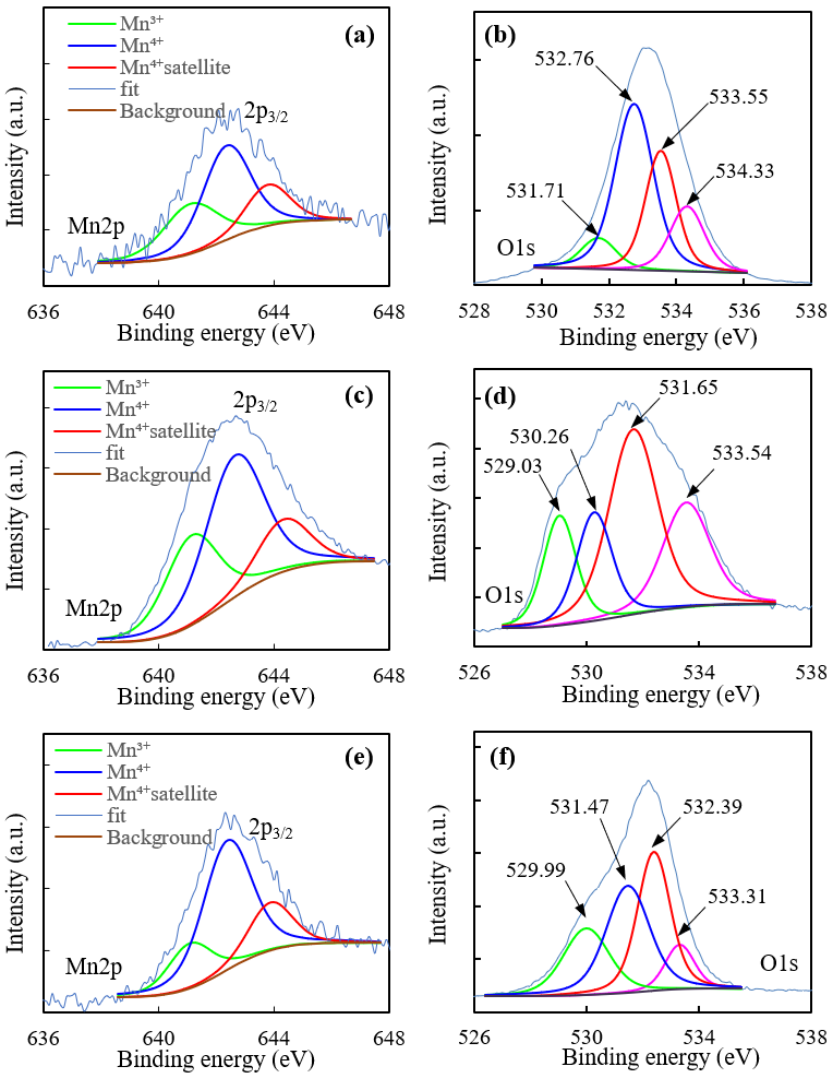


**Figure 6.** Mn2p and O1s XPS spectra for the $Mn_{91.1}Cu_{8.9}/SiO_2$–IWI (**a**,**b**); $Mn_{91.1}Cu_{8.9}/SiO_2$–UH (**c**,**d**); and $Mn_{89.9}Cu_{10.1}/SiO_2$–AE (**e**,**f**) catalysts calcined at 350 °C for 3.5 h.

Considering that the $Mn^{4+} / \sum_{n=0}^{4} Mn^{n+}$ ratio is not the only parameter determining the $NO_x$ conversion efficiency, both chemical and physical properties should be investigated to provide the proper and comprehensive explanation of the efficiency of the catalysts prepared.

Considering the O1s spectra (Figures 5 and 6) and the survey XPS spectra (not shown) describing all the elements existing in the catalysts, oxygen was found as a part of silicon dioxide (carrier), adventitious carbon (formed as a result of catalysts being exposed to ambient air), and oxides of Mn and Cu existing as lattice oxide/hydrated or defective oxide/adsorbed water and organic oxygen. The existence of Cu hydroxides and MnOOH can be excluded because of the calcination conducted at the temperature of 350 °C for 3.5 h, since according to [37] all MnOOH species should be converted to $MnO_2$ at the temperature of 300 °C, while $Cu(OH)_2$ species would be transformed to CuO in the temperature range of 155–170 °C [38].

### 2.1.4. XRD Analysis

Based on the XRD measurements it was determined that the active Mn species in the catalysts prepared by stepwise addition of a reducing agent, wet impregnation, urea hydrolysis and ammonia evaporation are rather amorphous than crystalline, since no sharp Bragg peaks were observed from the XRD patterns (see Figure 7).

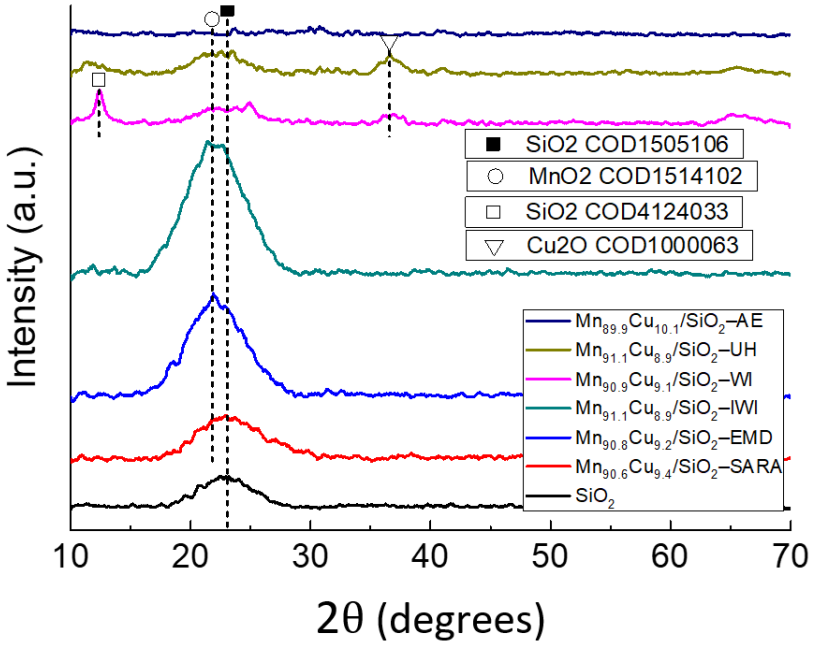


**Figure 7.** XRD patterns for the Mn–Cu oxide catalysts supported by the silica gel powder.

The characteristic $MnO_2$ peak was observed in the catalysts prepared by electroless metal deposition ($Mn_{90.8}Cu_{9.2}/SiO_2$–EMD) and incipient wetness impregnation ($Mn_{91.1}Cu_{8.9}/SiO_2$–IWI) methods. However, these peaks are quite broad, which can be related to stacking faults and other defects in a crystal structure. This means that even in these two catalysts there was no well-defined and organized crystal structure formed. Considering the Cu species, some crystalline phase was observed only for the $Mn_{90.9}Cu_{9.1}/SiO_2$–WI and the $Mn_{91.1}Cu_{8.9}/SiO_2$–UH catalysts, and again the observed peaks are quite broad meaning that there was no well-defined crystal structure even in these two mentioned catalysts. Therefore, generally all the Mn–Cu oxide catalysts prepared more likely can be assigned to the amorphous phase which is in agreement with the results of Tang et al. [39], where the unsupported $MnO_x$ catalysts were prepared by the rheological phase reaction method, low temperature solid phase reaction method and co-precipitation method and calcined at the temperature of 350 °C. In the same article [39], Tang et al. demonstrated that the amorphous phase is more active in regard to $NO_x$ conversion compared to the crystalline phase.

### *2.2. Catalytic Activity Test*

Since the loading provided by the active species deposited on the silica gel powder was different for different catalysts, the performance of catalysts in $NO_x$ conversion with ammonia was determined calculating both the absolute conversion efficiency obtained during the experiments and the conversion rate provided by 1 g of the active species deposited.

The catalyst prepared by the incipient wetness impregnation method ($Mn_{91.1}Cu_{8.9}/SiO_2$–IWI) characterized by the highest SSA and at the same time the lowest loading yielded the highest conversion rate related to 1 g of the active species deposited (Figure 8).

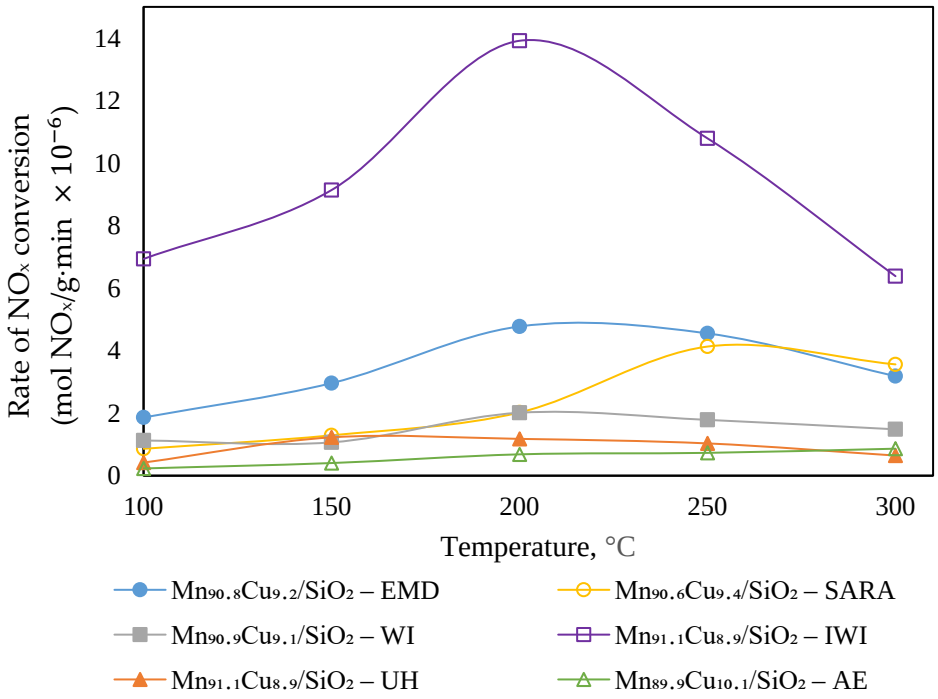


**Figure 8.** Rate of $NO_x$ conversion provided by the Mn–Cu oxide catalysts supported by the silica gel powder related to 1 g of the active species deposited: NO/$NH_3$ ratio ~1.0; NO ~300–500 ppm, $O_2$ ~3–5%; volumetric gas flow rate ~0.105 L· $min^{-1}$; GHSV ~450 $h^{-1}$; contact time—8 s.

Followed by this catalyst the highest rate of $NO_x$ conversion was provided by the $Mn_{90.8}Cu_{9.2}/SiO_2$–EMD and the $Mn_{90.6}Cu_{9.4}/SiO_2$–SARA catalysts, respectively, which can be correlated to the loading and SSA (see Table 2). The lower the loading, the lower the agglomeration, and consequently the higher the SSA. At the same time, at lower agglomeration and higher SSA, the higher $NO_x$ conversion provided by 1 g of the active species deposited can be supposed (the correlation coefficient between the loading and the $NO_x$ conversion provided by 1 g of the active species was −0.83). However, the SSA is not the only reason to explain the better $NO_x$ conversion provided by the $Mn_{90.8}Cu_{9.2}/SiO_2$–EMD catalyst compared to the $Mn_{90.6}Cu_{9.4}/SiO_2$–SARA catalyst. Both the catalysts showed almost the same rate of $NO_x$ reduction at the temperature range of 250–300 °C (see Figure 8), however the predominance of the former was obvious at lower temperatures. The $Mn_{90.8}Cu_{9.2}/SiO_2$–EMD catalyst was more effective than the $Mn_{90.6}Cu_{9.4}/SiO_2$–SARA at the temperatures of 100–200 °C even considering the absolute values of $NO_x$ reduction (see Figure 9), however the loading of the latter was higher. Therefore, considering both the physical properties and the catalytic performance, the $Mn_{90.8}Cu_{9.2}/SiO_2$–EMD catalyst can be considered as more attractive one. It can be supposed that the electroless metal deposition method provides better textural properties, which can be the reason to explain the predominance of the $Mn_{90.8}Cu_{9.2}/SiO_2$–EMD catalyst over the $Mn_{90.6}Cu_{9.4}/SiO_2$–SARA catalyst, since the difference in loading between these two catalysts is quite small (1.4% only) and the $Mn^{4+}$ / $\sum_{n=0}^{4} Mn^{n+}$ ratio was almost the same for both catalysts.

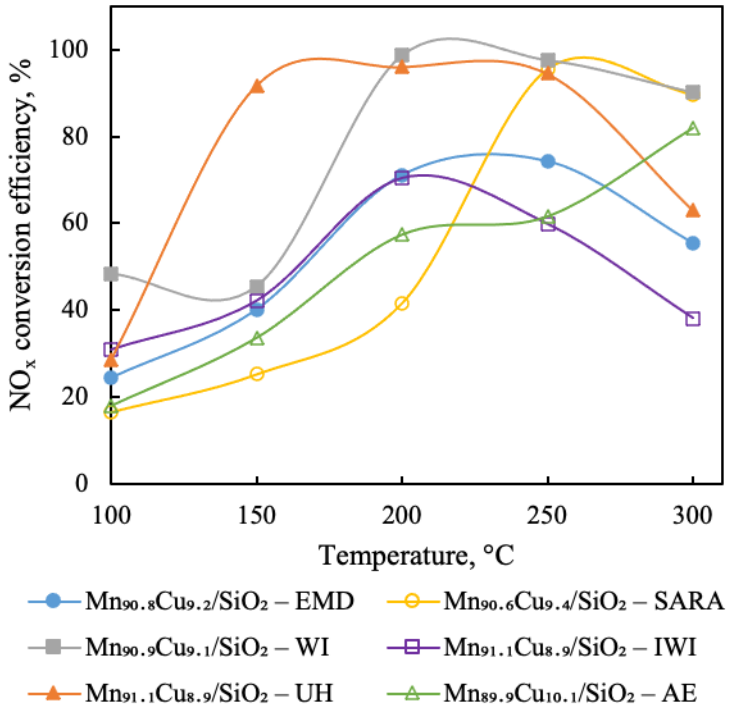


**Figure 9.** Catalytic performance of the Mn–Cu oxide catalysts supported by the silica gel powder for $NO_x$ conversion with ammonia: NO/$NH_3$ ratio ~1.0; NO ~300–500 ppm, $O_2$ ~3–5%; volumetric gas flow rate ~0.105 L· $min^{-1}$; GHSV ~450 $h^{-1}$; contact time—8 s.

The catalyst prepared by the incipient wetness impregnation ($Mn_{91.1}Cu_{8.9}/SiO_2$–IWI) was shown to be more effective than that prepared by the electroless metal deposition ($Mn_{90.8}Cu_{9.2}/SiO_2$–EMD) based on both the rate of $NO_x$ conversion related to 1 g of the active species deposited and the absolute values of $NO_x$ conversion. Although the absolute values of $NO_x$ conversion efficiency of the latter catalyst were higher in the temperature range of 200–300 °C, the difference is insignificant considering the loading of Mn and Cu species.

The lowest rate of $NO_x$ conversion related to 1 g of the active species was observed for the $Mn_{89.9}Cu_{10.1}/SiO_2$–AE catalyst characterized by the highest Mn and Cu loading and the lowest SSA. It can be concluded that the dispersion of catalytically active species plays the important role in the $NO_x$ conversion. With increasing the loading, the distribution of active species decreases, while the agglomeration and pores clogging increases causing the reduction in SSA and pore volume. Moreover, as a result of clogging the pores and agglomeration the amount of active species available for the catalytic reaction decreases significantly. Thus, as it has been assumed considering the textural properties and SEM images of the $Mn_{89.9}Cu_{10.1}/SiO_2$–AE catalyst, the ammonia evaporation method was shown to be ineffective, and it definitely cannot be considered as the optimal technique for preparation of $NH_3$-SCR de-$NO_x$ catalysts due to the agglomeration and extremely intensive clogging the pores.

The obvious advantage of the urea hydrolysis method for preparation of the $NH_3$-SCR de-$NO_x$ catalysts is the possibility to rich the high enough loading (up to 12 wt %) maintaining the relatively high SSA (up to 50 $m^2 \cdot g^{-1}$). However, considering both the absolute $NO_x$ conversion efficiency and the rate of $NO_x$ conversion related to 1 g of the active species deposited, it can be seen that the $Mn_{90.9}Cu_{9.1}/SiO_2$–WI catalyst was shown to be more effective than the $Mn_{91.1}Cu_{8.9}/SiO_2$–UH catalyst at all the temperatures investigated except for the temperature of 150 °C, although the latter possesses better textural properties, higher loading and almost the same $Mn^{4+} / \sum_{n=0}^{4} Mn^{n+}$ ratio. The high efficiency of the catalyst prepared by wet impregnation requires deeper investigation and

further understanding. Considering all the results obtained such methods as incipient wetness impregnation and wet impregnation can be considered as the most attractive techniques for preparation of $NH_3$-SCR de-$NO_x$ catalysts from all investigated in the present study.

## 3. Materials and Methods

### *3.1. Catalyst Preparation*

Mn–Cu–$O_x$/$SiO_2$ catalysts were prepared by six different methods: electroless metal deposition, stepwise addition of a reducing agent, wet impregnation, incipient wetness impregnation, urea hydrolysis, and ammonia evaporation. Mesoporous silica gel powder (silica gel 60, 0.063–0.1 mm, Merck, Darmstadt, Germany) was used as a support for deposition of Mn and Cu oxides.

#### 3.1.1. Electroless Metal Deposition

The electroless metal deposition technique is described in [40]. Prior to the active layer deposition, silica gel powder (30 mL) was activated in the 2.0 g·$L^{-1}$ $PdCl_2$ solution at the temperature of 25 °C for 1 min. This allows the formation of active sites on the carrier surface required for improved deposition of the active species and avoids or reduces bulk deposition. After the activation procedure, the support was rinsed with deionized water to remove all physisorbed chemical species. Cu and Mn catalytically active species were deposited on the activated support by sequential treatment of the latter in the Cu-plating and Mn-plating solutions, respectively. The composition of the Cu-plating solution was as follows: $CuSO_4$—0.01 mol· $L^{-1}$, $CH_2O$ (formaldehyde)—0.45 mol·$L^{-1}$, (ethylenedinitrilo)tetra-2-propanol—0.1 mol· $L^{-1}$, while the Mn-plating solution contained 0.25 mol· $L^{-1}$ $KMnO_4$ only. The residence time of the support in the Cu-plating and Mn-plating solutions was 1 h and 40 h, respectively. During the whole deposition process the support was vigorously stirred with a magnetic mixer. After the deposition was finished the support coated with the catalytically active Cu and Mn species was extracted from the metal-plating solution by a centrifugation, rinsed with the deionized water, dried under ambient conditions, and calcined at the temperature of 350 °C for 3.5 h. The prepared catalyst was denoted as MnCu/$SiO_2$–EMD.

#### 3.1.2. Stepwise Addition of a Reducing Agent

The principle of deposition of active species by stepwise addition of a reducing agent can be found elsewhere in the literature [27]. Sodium borohydride ($NaBH_4$) was applied as a reducing agent for deposition of the catalytically active Cu and Mn species. As in the electroless metal deposition the support was activated in the 2.0 g·$L^{-1}$ $PdCl_2$ solution prior to the deposition process. After the activation, 50 mL of the silica gel powder were sequentially treated in the Cu-plating (1 h) and the Mn-plating (24 h) solutions with the same composition as it has been mentioned previously. Vigorously stirring was maintained throughout the deposition process. The total amount of the sodium borohydride added to the metal-plating solutions of 500 mL each was 2 g. During the deposition of Cu species 0.5 g of $NaBH_4$ was divided by three equal portions and added to the solution in the beginning of the deposition procedure, after the 15 min and after the 30 min of deposition, while 1.5 g of $NaBH_4$ was added to the Mn-plating solution during the deposition of Mn species by ca. 0.2 g every 30 min. After getting the deposition completed the active Cu and Mn species supported be the silica gel powder were extracted from the metal-plating solution by a centrifugation, rinsed with the deionized water, dried under ambient conditions, and calcined at the temperature of 350 °C for 3.5 h. The prepared catalyst was denoted as MnCu/$SiO_2$–SARA.

#### 3.1.3. Wet Impregnation

The basis of the wet impregnation method can be found elsewhere in the literature [27]. The silica gel powder in the amount of 50 mL was sequentially treated in 0.01M $CuSO_4$ and

0.25M $KMnO_4$ solutions of 500 mL each for 3 h and 40 h, respectively under the vigorous stirring with a magnetic mixer. After the deposition, the suspension was centrifuged to separate the catalyst from the liquid phase, followed by rinsing the former with the deionized water, drying under ambient conditions and calcination at the temperature of 350 °C for 3.5 h. The prepared catalyst was denoted as $MnCu/SiO_2$–WI.

#### 3.1.4. Incipient Wetness Impregnation

The general description of the incipient wetness impregnation technique can be found in [41]. Prior to the deposition process the silica gel powder in the amount of 45 g was dried in the oven at the temperature of 120 °C for 1 h. For the deposition of active species, the solution containing 0.02 mol· $L^{-1}$ $CuSO_4$ and 0.3 mol· $L^{-1}$ $KMnO_4$ was used. Based on the pore volume of the support determined by $N_2$ adsorption (0.8 $cm^3 \cdot g^{-1}$) the volume of the solution required for deposition was calculated to be 36 mL. The deposition process was conducted under intensive mixing and as a result the solution was completely adsorbed by the support. After that, the support with the deposited active species was dried under ambient conditions and calcined at the temperature of 350 °C for 3.5 h. The prepared catalyst was denoted as $MnCu/SiO_2$–IWI.

#### 3.1.5. Urea Hydrolysis

The principle deposition by urea hydrolysis can be found in [28]. For the deposition of active species 500 mL of the solution containing 0.01 mol· $L^{-1}$ $CuSO_4$ and 0.25 mol· $L^{-1}$ $KMnO_4$ were prepared, and the pH was adjusted to 3 by means of $HNO_3$. After that 100 mL of the silica gel powder and 45 g of the urea ($CH_4N_2O$) were added to the solution with the following heating the latter to 90 °C and vigorous stirring. Under such conditions the deposition process was conducted for 12 h (until the pH 7 was achieved). The support with the deposited Cu and Mn species was extracted from the solution by a centrifugation, rinsed with the deionized water, dried under ambient conditions, and calcined at the temperature of 350 °C for 3.5 h. The prepared catalyst was denoted as $MnCu/SiO_2$–UH.

#### 3.1.6. Ammonia Evaporation

The principle of ammonia evaporation method can be found in [28]. For the deposition of active species 500 mL of the solution containing 0.01 mol· $L^{-1}$ $CuSO_4$, 0.25 mol· $L^{-1}$ $KMnO_4$ and 0.1 mol· $L^{-1}$ $K_2CO_3$ were prepared, and the pH was adjusted to 11 by adding 150 mL of the $NH_4OH$. After that 100 mL of the silica gel powder were added to the solution followed by heating the latter to 90 °C under vigorous stirring. Under such conditions the deposition process was conducted for 12 h (until the pH value was changed from 11 to 8). The silica gel powder with the deposited Cu and Mn species was extracted from the solution by a centrifugation, rinsed with the deionized water, dried under ambient conditions, and calcined at the temperature of 350 °C for 3.5 h. The prepared catalyst was denoted as $MnCu/SiO_2$–AE.

### *3.2. Catalyst Characterization*

Composition of the catalytic layer deposited on the surface of the silica gel powder and the loading (wt%) of the active metals (Mn and Cu) being part of the catalytic layer were determined by inductively coupled plasma optical emission spectroscopy (ICP-OES) with the ICP optical emission spectrometer Optima 7000DV (Perkin Elmer, Waltham, MA, USA). To investigate the morphology of the Mn–Cu–$O_x$ catalytic layer supported by the silica gel powder and the dispersion of the active species on the surface of the catalysts prepared SEM images and EDX elemental mapping were provided by means of the scanning electron microscope TM4000Plus (Hitachi). The oxidation states of the main active species being part of the catalytic layer were determined by X-ray photoelectron spectroscopy (XPS) using ESCALAB MK II spectrometer (VG Scientific, East Grinstead, UK) equipped with a Mg K$\alpha$ X-ray radiation source (1253.6 eV) operated at 300 W with the fixed pass energy of 20 eV. The pressure of $10^{-7}$ Pa was kept in an UHV analysis chamber. X-ray diffraction

(XRD) measurements were conducted using X-ray diffractometer D2 Phaser (Bruker AXS, Billerica, MA, USA) to provide comprehensive information about the structure of the active species deposited on the surface of the amorphous silica gel powder. XRD patterns were recorded using Cu Kα radiation. A step-scan mode was used in the 2θ range from 10° to 70° with the step length of 0.04° and the counting time of 1 s per step. Additionally, the specific surface area (SSA), total pore volume, pore distribution and the average pore size of both the carrier used and the supported catalysts were determined by means of nitrogen adsorption at −196 °C using the Micromeritics TriStar II 3020 analyzer. The Brunauer–Emmett–Teller model was used to calculate the specific surface area. Before measurements, all the samples were degassed in a nitrogen atmosphere at 100 °C for 2 h.

### *3.3. Catalytic Activity Test ($NH_3$-SCR de-$NO_x$)*

The prepared Mn–Cu oxide catalysts supported by the silica gel powder (0.063–0.1 mm) were tested for the SCR de-$NO_x$ by ammonia using the experimental setup presented in Figure 10. Three separate gas mixtures NO(1500 ppm)/$N_2$, $NH_3$(1500 ppm)/$N_2$ and $O_2$ (vol. 9%)/$N_2$ were supplied from three gas cylinders into the setup through mass flow controllers, creating the resulting gas mixture with NO/$NH_3$ ratio of ~1.0 and concentrations of the main gas components of ca. 300–500 ppm, ca. 300–500 ppm and ca. 3–5% for NO, $NH_3$, and $O_2$, respectively. The catalysts were investigated as a fixed bed at GHSV of 450 $h^{-1}$ and the $NO_x$ conversion efficiency was expressed as both the absolute conversion rate achieved and the rate of $NO_x$ conversion provided by 1 g of the catalytically active species deposited. The volumetric flow rate of the resulting gas mixture passing through the catalysts under such operating conditions was about 0.105 L· $min^{-1}$. Additionally, the catalyst provided the highest SCR performance was tested as a fluidized bed under bubbling fluidization conditions at GHSV of 940 $h^{-1}$ (volumetric gas flow rate of 0.219 L· $min^{-1}$). Catalytic activity tests were conducted in the temperature range of 100–300 °C (low-temperature conditions). $NO_x$ (NO and $NO_2$) concentrations were measured prior to and after the catalysts using the TESTO 350XL gas analyzer (Testo, Germany).

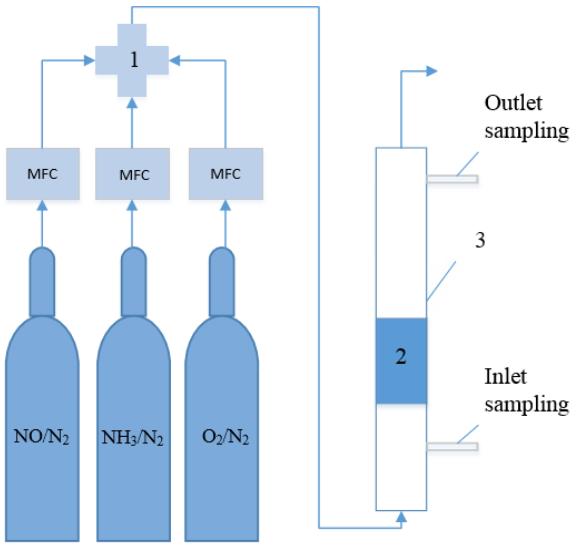


**Figure 10.** Schematic view of the experimental setup: MFC—mass flow controller; 1—gas collector; 2—catalyst; 3—catalytic reactor.

## 4. Conclusions

It was shown that a preparation method has a significant impact on both the physicochemical properties and the catalytic performance of the catalysts. A method applied for preparation of SCR de-$NO_x$ catalysts affects the morphology, oxidation state of the active species, and textural properties, in particular specific surface area, total pore volume and pore size distribution. Using the silica gel powder as a carrier it was shown that the

incipient wetness impregnation is the only method that ensures the remaining of initial size of the support, while other techniques where the significant amount of liquid solutions was used to prepare the catalysts resulted in segmentation of the silica gel. Although the carrier used for the deposition of the active species is a highly porous material, all the methods applied for preparation of catalysts provided the uniform distribution of the main active component—Mn, while some nonuniformity was observed for the doping element—Cu. Considering both the rate of $NO_x$ conversion related to 1 g of the active species deposited and the absolute values of $NO_x$ conversion, and taking into account the loading provided by the active catalytic species the most attractive method for preparation of SCR de-$NO_x$ catalysts is supposed to be incipient wetness impregnation. Additional advantages of this preparation method are its simplicity and low amount of precursor solution required for deposition of active species. Moreover, this technique is fast, there is no need for additional chemicals apart from Mn and Cu precursors and rinsing the catalyst after the deposition is not required.

**Author Contributions:** Investigation, D.U.; writing—original draft preparation, D.U.; writing—review and editing, D.U. and E.B.-G.; visualization, D.U.; supervision, E.B.-G. All authors have read and agreed to the published version of the manuscript.

**Funding:** Financial support received from the projects "Development of doctoral studies" (Project Code S0802KDO14) and "Centre for environmentally friendly construction, composite materials and environmental technologies" is acknowledged (EU structural funds; Project Nr. 01.2.2-CPVA-K-703-02-0031).

**Acknowledgments:** The main supervision provided by the Habil. Pranas Baltrėnas who passed away due to COVID-19 infection was highly relevant and gratefully acknowledged.

**Conflicts of Interest:** The authors declare no conflict of interest. The funders had no role in the design of the study; in the collection, analyses, or interpretation of data; in the writing of the manuscript, or in the decision to publish the results.

## References

1. Cheng, X.; Bi, X.T. A review of recent advances in selective catalytic $NO_x$ reduction reactor technologies. *Particuology* **2014**, *16*, 1–18. [CrossRef]
2. European Environment Agency. *Air Quality in Europe—2019 Report*; Publications Office of the European Union: Luxembourg, 2019.
3. United States Environmental Protection Agency. Nitrogen Dioxide ($NO_2$) Pollution. Available online: https://www.epa.gov/no2-pollution/basic-information-about-no2#Effects (accessed on 10 April 2021).
4. Zhao, G.; Li, M.; Wang, L.; Wang, D.; Liang, J.; Xue, G. Environmentally-friendly tourmaline modified $CeMnFeO_x$ catalysts for low-temperature selective catalytic reduction of $NO_x$ with $NH_3$. *Catal. Today* **2020**, *355*, 385–396. [CrossRef]
5. Chen, L.; Si, Z.; Wu, X.; Weng, D.; Ran, R.; Yu, J. Rare earth containing catalysts for selective catalytic reduction of $NO_x$ with ammonia: A review. *J. Rare Earths* **2014**, *32*, 907–917. [CrossRef]
6. Pu, Y.; Xie, X.; Jiang, W.; Yang, L.; Jiang, X.; Yao, L. Low-temperature selective catalytic reduction of $NO_x$ with $NH_3$ over zeolite catalysts: A review. *Chin. Chem. Lett.* **2020**, *31*, 2549–2555. [CrossRef]
7. Li, J.; Chang, H.; Ma, L.; Hao, J.; Yang, R.T. Low-temperature selective catalytic reduction of $NO_x$ with $NH_3$ over metal oxide and zeolite catalysts-A review. *Catal. Today* **2011**, *175*, 147–156. [CrossRef]
8. Sorrels, J.L.; Randall, D.D.; Schaffner, K.S.; Fry, C.R. Chapter 2 Selective Catalytic Reduction. In *EPA Air Pollution Control Cost Manual*; US EPA: Research Triangle Park, NC, USA, 2019; ISBN 1070-9908.
9. Kang, M.; Park, E.D.; Kim, J.M.; Yie, J.E. Manganese oxide catalysts for $NO_x$ reduction with $NH_3$ at low temperatures. *Appl. Catal. A Gen.* **2007**, *327*, 261–269. [CrossRef]
10. Liu, C.; Shi, J.W.; Gao, C.; Niu, C. Manganese oxide-based catalysts for low-temperature selective catalytic reduction of $NO_x$ with $NH_3$: A review. *Appl. Catal. A Gen.* **2016**, *522*, 54–69. [CrossRef]
11. Ettireddy, P.R.; Ettireddy, N.; Mamedov, S.; Boolchand, P.; Smirniotis, P.G. Surface characterization studies of $TiO_2$ supported manganese oxide catalysts for low temperature SCR of NO with $NH_3$. *Appl. Catal. B Environ.* **2007**, *76*, 123–134. [CrossRef]
12. Gao, C.; Shi, J.W.; Fan, Z.; Gao, G.; Niu, C. Sulfur and water resistance of Mn-based catalysts for low-temperature selective catalytic reduction of $NO_x$: A review. *Catalysts* **2018**, *8*, 11. [CrossRef]
13. Li, Y.; Wan, Y.; Li, Y.; Zhan, S.; Guan, Q.; Tian, Y. Low-temperature selective catalytic reduction of NO with $NH_3$ over $Mn_2O_3$-doped $Fe_2O_3$ hexagonal microsheets. *ACS Appl. Mater. Interfaces* **2016**, *8*, 5224–5233. [CrossRef]
14. Zhang, N.; He, H.; Wang, D.; Li, Y. Challenges and opportunities for manganese oxides in low-temperature selective catalytic reduction of $NO_x$ with $NH_3$: $H_2O$ resistance ability. *J. Solid State Chem.* **2020**, *289*, 121464. [CrossRef]

15. Kang, M.; Park, E.D.; Kim, J.M.; Yie, J.E. Cu-Mn mixed oxides for low temperature NO reduction with $NH_3$. *Catal. Today* **2006**, *111*, 236–241. [CrossRef]
16. Tang, X.; Hao, J.; Yi, H.; Li, J. Low-temperature SCR of NO with $NH_3$ over AC/C supported manganese-based monolithic catalysts. *Catal. Today* **2007**, *126*, 406–411. [CrossRef]
17. Tian, W.; Yang, H.; Fan, X.; Zhang, X. Catalytic reduction of $NO_x$ with $NH_3$ over different-shaped $MnO_2$ at low temperature. *J. Hazard. Mater.* **2011**, *188*, 105–109. [CrossRef]
18. Yu, J.; Guo, F.; Wang, Y.; Zhu, J.; Liu, Y.; Su, F.; Gao, S.; Xu, G. Sulfur poisoning resistant mesoporous Mn-base catalyst for low-temperature SCR of NO with $NH_3$. *Appl. Catal. B Environ.* **2010**, *95*, 160–168. [CrossRef]
19. Zamudio, M.A.; Russo, N.; Fino, D. Low temperature $NH_3$ selective catalytic reduction of $NO_x$ over substituted $MnCr_2O_4$ spinel-oxide catalysts. *Ind. Eng. Chem. Res.* **2011**, *50*, 6668–6672. [CrossRef]
20. Zuo, J.; Chen, Z.; Wang, F.; Yu, Y.; Wang, L.; Li, X. Low-temperature selective catalytic reduction of $NO_x$ with $NH_3$ over novel Mn-Zr mixed oxide catalysts. *Ind. Eng. Chem. Res.* **2014**, *53*, 2647–2655. [CrossRef]
21. Camposeco, R.; Castillo, S.; Rodríguez-González, V.; García-Serrano, L.A.; Mejía-Centeno, I. Selective catalytic reduction of $NO_x$ by $NH_3$ at low temperature over manganese oxide catalysts supported on titanate nanotubes. *Chem. Eng. Commun.* **2018**, *205*, 1583–1593. [CrossRef]
22. Snapkauskiene, V.; Valinčius, V.; Grigaitiene, V. Preparation and characterization of $TiO_2$-based plasma-sprayed coatings for $NO_x$ abatement. *Catal. Today* **2012**, *191*, 154–158. [CrossRef]
23. Salazar, M.; Becker, R.; Grünert, W. Hybrid catalysts-an innovative route to improve catalyst performance in the selective catalytic reduction of NO by $NH_3$. *Appl. Catal. B Environ.* **2015**, *165*, 316–327. [CrossRef]
24. Sun, P.; Guo, R.T.; Liu, S.M.; Wang, S.X.; Pan, W.G.; Li, M.Y. The enhanced performance of $MnO_x$ catalyst for $NH_3$-SCR reaction by the modification with Eu. *Appl. Catal. A Gen.* **2017**, *531*, 129–138. [CrossRef]
25. Gao, F.; Tang, X.; Yi, H.; Zhao, S.; Li, C.; Li, J.; Shi, Y.; Meng, X. A review on selective catalytic reduction of $NO_x$ by $NH_3$ over Mn–based catalysts at low temperatures: Catalysts, mechanisms, kinetics and DFT calculations. *Catalysts* **2017**, *7*, 199. [CrossRef]
26. Zhang, S.; Zhang, B.; Liu, B.; Sun, S. A review of Mn-containing oxide catalysts for low temperature selective catalytic reduction of $NO_x$ with NH3: Reaction mechanism and catalyst deactivation. *RSC Adv.* **2017**, *7*, 26226–26242. [CrossRef]
27. Li, H.; Ban, L.; Wang, Z.; Meng, P.; Zhang, Y.; Wu, R.; Zhao, Y. Regulation of Cu species in $CuO/SiO_2$ and its structural evolution in ethynylation reaction. *Nanomaterials* **2019**, *9*, 842. [CrossRef] [PubMed]
28. Bezemer, G.L.; Radstake, P.B.; Koot, V.; van Dillen, A.J.; Geus, J.W.; de Jong, K.P. Preparation of Fischer-Tropsch cobalt catalysts supported on carbon nanofibers and silica using homogeneous deposition-precipitation. *J. Catal.* **2006**, *237*, 291–302. [CrossRef]
29. Alothman, Z.A. A review: Fundamental aspects of silicate mesoporous materials. *Materials* **2012**, *5*, 2874–2902. [CrossRef]
30. Chakraborty, A.; Sun, B. An adsorption isotherm equation for multi-types adsorption with thermodynamic correctness. *Appl. Therm. Eng.* **2014**, *72*, 190–199. [CrossRef]
31. Guo, B.; Shen, H.; Shu, K.; Zeng, Y.; Ning, W. The study of the relationship between pore structure and photocatalysis of mesoporous $TiO_2$. *J. Chem. Sci.* **2009**, *121*, 317–321. [CrossRef]
32. Oku, M.; Hirokawa, K.; Ikeda, S. X-ray photoelectron spectroscopy of manganese-oxygen systems. *J. Electron Spectros. Relat. Phenom.* **1975**, *7*, 465–473. [CrossRef]
33. Nesbitt, H.W.; Banerjee, D. Interpretation of XPS Mn(2p) spectra of Mn oxyhydroxides and constraints on the mechanism of $MnO_2$ precipitation. *Am. Mineral.* **1998**, *83*, 305–315. [CrossRef]
34. Biesinger, M.C.; Payne, B.P.; Grosvenor, A.P.; Lau, L.W.M.; Gerson, A.R.; Smart, R.S.C. Resolving surface chemical states in XPS analysis of first row transition metals, oxides and hydroxides: Cr, Mn, Fe, Co and Ni. *Appl. Surf. Sci.* **2011**, *257*, 2717–2730. [CrossRef]
35. Langell, M.A.; Hutchings, C.W.; Carson, G.A.; Nassir, M.H. High resolution electron energy loss spectroscopy of MnO(100) and oxidized MnO(100). *J. Vac. Sci. Technol. A Vac. Surf. Film* **1996**, *14*, 1656–1661. [CrossRef]
36. Yao, X.; Ma, K.; Zou, W.; He, S.; An, J.; Yang, F.; Dong, L. Influence of preparation methods on the physicochemical properties and catalytic performance of $MnO_x$-$CeO_2$ catalysts for $NH_3$-SCR at low temperature. *Chin. J. Catal.* **2017**, *38*, 146–159. [CrossRef]
37. González, C.; Gutiérrez, J.I.; Gonzalez-Velasco, J.R.; Cid, A.; Arranz, A.; Arranz, J.F. Transformations of manganese oxides under different thermal conditions. *J. Therm. Anal.* **1996**, *47*, 93–102. [CrossRef]
38. Fukuda, M.; Koga, N. Kinetics and mechanisms of the thermal decomposition of copper(II) hydroxide: A consecutive process comprising induction period, surface reaction, and phase boundary-controlled reaction. *J. Phys. Chem. C* **2018**, *122*, 12869–12879. [CrossRef]
39. Tang, X.; Hao, J.; Xu, W.; Li, J. Low temperature selective catalytic reduction of $NO_x$ with $NH_3$ over amorphous $MnO_x$ catalysts prepared by three methods. *Catal. Commun.* **2007**, *8*, 329–334. [CrossRef]
40. Norkus, E.; Tamašauskaite-Tamašiunaite, L. Application of electroless metal deposition and galvanic displacement for fabrication of catalysts for borohydride oxidation. In *Encyclopedia of Interfacial Chemistry: Surface Science and Electrochemistry*; Elsevier: Amsterdam, The Netherlands, 2018; pp. 361–372. ISBN 9780128098943.
41. Munnik, P.; de Jongh, P.E.; de Jong, K.P. Recent developments in the synthesis of supported catalysts. *Chem. Rev.* **2015**, *115*, 6687–6718. [CrossRef]